

Speeding up Local Optimization in Vehicle Routing with Tensor-based GPU Acceleration

Zhenyu Lei^a, Jin-Kao Hao^{a,*}

^a*LERIA, Université d'Angers, 2 Boulevard Lavoisier, 49045 Angers, France*

Qinghua Wu^b

^b*School of Management, Huazhong University of Science and Technology, No.1037, Luoyu Road, Wuhan, China*

Abstract

Local search plays a central role in many effective heuristic algorithms for the vehicle routing problem (VRP) and its variants. However, neighborhood exploration is known to be computationally expensive and time consuming, especially for large instances or problems with complex constraints. In this study, we explore a promising direction to address this challenge by introducing an original tensor-based GPU acceleration method designed to speed up the commonly used local search operators in vehicle routing. By using an attribute-based representation, the method offers broad extensibility, making it applicable to different VRP variants. Its low-coupling architecture, with intensive computations completely offloaded to the GPU, ensures seamless integration in various local search-based algorithms and frameworks, leading to significant improvements in computational efficiency and potentially improved solution quality. Through comparative experiments on benchmark instances of three routing problems, we demonstrate the substantial computational advantages of the proposed approach over traditional CPU-based implementations. We also provide a detailed analysis of the strengths and limitations of the method, providing valuable insights into its performance characteristics and identifying potential bottlenecks in practical applications. These findings contribute to a better understanding and suggest directions for future improvements.

Keywords: Tensor-based GPU acceleration; Local search; Vehicle routing.

* Corresponding author.

Email addresses: zhenyu.lei@etud.univ-angers.fr (Zhenyu Lei), jin-kao.hao@univ-angers.fr (Jin-Kao Hao), qinghuawu1005@gmail.com (Qinghua Wu).

1 Introduction

The Vehicle Routing Problem (VRP) [1,2] is one of the most well-known combinatorial optimization problems and is very computationally challenging due to its NP-hard nature [3]. The VRP involves dispatching a fleet of vehicles to serve a set of customers, with each route starting and ending at a depot, while satisfying certain constraints and minimizing the total operational cost. As a fundamental problem in combinatorial optimization, the VRP finds numerous real-world applications in the fields of transportation, logistics, supply chain management, and so on.

Since its introduction, the VPR and its variants have been studied extensively in the literature for over decades. Among the many methods developed to solve these routing problems are exact, approximate, heuristic, and metaheuristic approaches. Due to the high complexity of the routing problems, exact and approximate methods [4–6] are typically used to deal with small and medium problem instances. For large instances, heuristic and metaheuristic methods remain the main approach used to find good enough suboptimal solutions within a reasonable time, making them more applicable in practice. These include techniques such as simulated annealing [7,8], tabu search [9,10], genetic algorithms [11,12], and memetic algorithms [13,14], among others. Comprehensive literature reviews on the classification of VRPs and the existing methods can be found in surveys [15–18].

To meet the requirements of real-world scenarios, the size and complexity of the studied VRPs have been increasing. Despite extensive efforts to solve these complex VRPs, computational efficiency remains a major challenge, especially for the VRPs with complex constraints. Local search, a core component of many VRP solution algorithms, requires iterative exploration of solution neighborhoods to improve solution quality. However, neighborhood evaluation in local search is computationally intensive and time consuming, especially when dealing with large instances or intricate constraints. Therefore, to increase the search and computational performance of the algorithm, it is essential to improve the efficiency of neighborhood evaluation.

With recent advances in computer hardware, GPU (Graphics Processing Unit) [19] has become increasingly promising for accelerating computationally intensive tasks in combinatorial optimization. With their highly parallel architecture and thousands of cores, GPUs are well suited for large-scale data processing and tasks requiring extensive parallelism, offering significant speedups over traditional CPU-based approaches for solving complex optimization problems.

[20] implemented classic heuristics such as hill climbing and simulated annealing on GPUs, using the Graph Partitioning Problem as a tested problem. Their

results showed significant speedups compared to CPU-based implementations. [21] reviewed several GPU-based genetic algorithms (GAs), examining various parallel GA models, including Master-Slave, Island, and Cellular, across different levels of parallelism, such as chromosome-level and gene-level granularity. [22,23] proposed parallel hybrid evolutionary algorithms to solve the partial Latin square extension problem and the unconstrained binary quadratic problem. Their approach implemented an algorithmic-level parallelism by running multiple local search processes in parallel within a large population on the GPU, fully exploiting the GPU parallelism. [24] developed a GPU-based tabu search algorithm for the maximum diversity problem. By introducing efficient data structures and local search strategies, they achieved significant speedups for neighborhood evaluation on GPU.

Several recent studies have also explored the use of GPUs to solve vehicle routing problems, which can be classified into two categories: coarse-grained parallelism, which accelerates high-level algorithmic components, and fine-grained parallelism, which focuses on speeding up neighborhood evaluation in local search.

[25] proposed a hybrid genetic algorithm integrating 2-opt local search to solve the capacitated VRP on GPU. The GPU was used to handle all algorithmic components, including population initialization, reproduction, 2-opt local search, and refining processes. [26] developed a GPU-based multi-objective memetic algorithm for the VRP with route balancing. They proposed two schemes for the parallelism: solution-level parallelism, where multiple solutions were processed using parallel local search, and route-level parallelism, which provided a finer granularity by parallelizing route level evaluations. However, their method did not exploit the finer node-level parallelism commonly used in neighborhood evaluations.

[27] explored GPU-based parallelization of 2-opt and 3-opt local search operators for the CVRP, achieving significant speedups over CPU implementations. Similarly, [28] extended GPU-based local search for the CVRP by incorporating additional operators such as or-opt, swap, and relocate, achieving comparable improvements in computational performance. However, their methods were limited to the basic travel distance evaluation. [29] addressed the single VRP with deliveries and selective pickups using a GPU-based variable neighborhood search, where the GPU was also tasked with parallel neighborhood evaluations. Despite incorporating multiple local search operators, their approach primarily optimized the evaluation of travel distance and struggled to effectively manage complex constraints.

These studies demonstrate the potential of GPU acceleration for solving VRPs. However, most existing methods are limited to basic VRP variants or simple search operators, with less focus on handling complex constraints or adapt-

ing to diverse VRP types. Furthermore, current approaches rely heavily on CUDA programming, which, while powerful, requires management of complex aspects such as data transfer, memory access, parallelism control, and thread synchronization, making it difficult for broader adoption.

In this study, we aim to fill the gap and propose a tensor-based GPU acceleration (TGA) method in a fine-grained manner to improve the computational efficiency of local search-based algorithms for solving complex VRPs. The main contributions of this study are as follows: (1) We present the first innovative tensor-based GPU acceleration method that can be embedded in local search algorithms for solving various VRPs. (2) The approach is highly extensible and adaptable, allowing easy application to a wide range of VRP variants with various attributes and easy integration into different VRP frameworks. (3) The tensor-based representation can be easily implemented using rich libraries and tools such as PyTorch and TensorFlow, making it accessible to a wide audience. (4) We conduct comparative experiments to evaluate the performance of the proposed TGA method against traditional CPU-based implementations. The results demonstrate significant improvements in both computational efficiency and solution quality, particularly for large-scale problem instances. (5) The in-depth theoretical and experimental analysis of the proposed TGA method offers valuable insights into its performance characteristics and reveals potential bottlenecks in practical applications. This analysis lays a solid basis for its applications in future research.

To examine the performance of the proposed method on different VRP variants and to illustrate its extensibility, we apply it to three popular routing problems: Capacitated VRP (CVRP), VRP with Time Windows (VRPTW), and VRP with Simultaneous Pickup and Delivery and Time Windows (VRP-SPDTW). Computational results on benchmark instances suggest that the method is adaptable and effective in handling diverse problem characteristics, and shows significant efficiency gains over traditional CPU-based implementations.

The rest of this paper is organized as follows. Section 2 provides a formal definition of VRPs. Section 3 introduces essential background on attribute representation and sequence concatenation-based move evaluation. Section 4 presents the proposed tensor-based GPU acceleration method. Section 5 shows computational results on benchmark instances to demonstrate the interest of the method, along with an in-depth analysis of its advantages and limitations. Section 6 discusses the extensibility and limitations of the proposed method. Section 7 gives concluding comments and suggests possible directions for future research.

2 Problem definition

This section introduces the three typical routing problems that serve as the case studies: the Capacitated VRP (CVRP), the VRP with Time Windows (VRPTW), and the VRP with Simultaneous Pickup and Delivery and Time Windows (VRPSPDTW). The VRPSPDTW is a generalization of both the CVRP and the VRPTW. Therefore, we will focus on defining the VRP-SPDTW, while showing how it is reduced to these more specific problems.

All three problems can be defined on a complete graph $\mathcal{G} = (\mathcal{V}, \mathcal{E})$, where the vertices or nodes $\mathcal{V} = \{v_0, v_1, \dots, v_{\mathcal{N}}\}$ represent the depot v_0 and the \mathcal{N} customers $\{v_1, \dots, v_{\mathcal{N}}\}$. The edges $\mathcal{E} = \{e_{ij} | v_i, v_j \in \mathcal{V}\}$ represent the connections between these nodes. Each customer node $v_i \in \mathcal{V}$ ($i \neq 0$) is associated with a delivery demand d_i and a pickup demand p_i . This means that the vehicle must deliver d_i units of goods from the depot v_0 to v_i and pick up p_i units from v_i back to the depot. Furthermore, each node v_i has a time window $[e_i, l_i]$ and a service time s_i , which specifies the earliest and latest time for the service, as well as the time spent at node v_i for the service. The depot has a time window $[e_0, l_0]$, specifying the earliest departure and latest return time, with its service time s_0 set to 0. Additionally, each edge $e_{ij} \in \mathcal{E}$ is associated with a travel distance c_{ij} and a travel time t_{ij} . For the VRPTW and the CVRP, the pickup demand $p_i = 0$, and moreover, the CVRP does not consider time-related attributes such as travel time, service time, or time windows.

A fleet of M homogeneous vehicles, each with a capacity \mathcal{Q} , serves all customers, starting and ending at the depot v_0 , while satisfying various constraints, including capacity and time windows. A solution S is represented as a set of closed routes $S = \{R_1, \dots, R_M\}$, where each route R_i consists of a sequence of nodes $\{n_{i,0}, n_{i,1}, \dots, n_{i,\mathcal{L}_i}, n_{i,\mathcal{L}_i+1}\}$ visited by the i -th vehicle. Here, $n_{i,j}$ denotes the j -th node in route R_i and \mathcal{L}_i is the number of served customers in that route. Thus, the length of route R_i is $|R_i| = \mathcal{L}_i + 2$. Note that both the first and last nodes in route R_i are the depot v_0 (i.e., $n_{i,0} = v_0$ and $n_{i,\mathcal{L}_i+1} = v_0$). To ensure that the load of each vehicle does not exceed its capacity \mathcal{Q} , the condition $q_{n_{i,j}} < \mathcal{Q}$ must hold for all $n_{i,j} \in R_i$, where $q_{n_{i,j}}$ represents the load of the i -th vehicle after visiting node $n_{i,j}$. For variants that incorporate time windows, let $a_{n_{i,j}}$ denote the arrival time at node $n_{i,j}$. Arriving before $e_{n_{i,j}}$ results in a wait time of $w_{n_{i,j}} = \max\{e_{n_{i,j}} - a_{n_{i,j}}, 0\}$, while arriving after $l_{n_{i,j}}$ renders the route infeasible.

$$\begin{aligned}
& \text{Minimize} && f(S) = \mu_1 \cdot M + \mu_2 \cdot D(S) && (1) \\
& \text{Subject to} && D(S) = \sum_{i=1}^M \sum_{j=0}^{\mathcal{L}_i} c_{n_{i,j}n_{i,j+1}} \\
& && S = \{R_1, \dots, R_M\} \\
& && R_i = \{n_{i,0}, n_{i,1}, \dots, n_{i,\mathcal{L}_i}, n_{i,\mathcal{L}_i+1}\}, \quad i = 1, \dots, M
\end{aligned}$$

Typically, we can describe the objective function of these problems as minimizing the total cost, which is the weighted sum of the number of vehicles and the travel distance with predefined weights, as shown in Equation (1), where μ_1 and μ_2 represent the costs or weights assigned to the vehicle dispatching and the travel distance, respectively.

3 Attribute representation and move evaluation

Efficient move evaluation is a critical step in the search process of local search algorithms and directly affects both solution quality and search efficiency. Our proposed tensor-based GPU acceleration (TGA) method uses an attribute-based solution representation and conceptualizes common local search move operators, such as *Relocate*, *Swap*, *2-opt**, and *2-opt*, as the concatenation of multiple route subsequences [30–32], allowing efficient evaluation of neighborhoods with respect to both the objective function and the constraints.

3.1 Matrix-based attribute representation

For an efficient move evaluation of local search operators, we propose to use attribute matrices to store the attribute values. Specifically, for each route, we define a matrix for each attribute to store the precomputed values of subsequences to facilitate the computation for concatenated sequences. Figure 1 illustrates an attribute matrix for a route with $|R| = 10$, where a_{ij} represents the attribute value for the subsequence from the i -th node to the j -th node in the route. For example, in the case of the travel distance attribute, a_{ij} is the total travel distance between the i -th node and the j -th node in the route. Note that only the upper triangular part of the matrix holds valid attribute values. These precomputed attributes are tailored to specific problem settings and constraints, providing strong adaptability across various VRP variants.

Using this matrix-based attribute representation, fast move evaluation can be achieved by performing sequence concatenation operations, which serves

a_{00}	a_{01}	a_{02}	a_{03}	a_{04}	a_{05}	a_{06}	a_{07}	a_{08}	a_{09}
	a_{11}	a_{12}	a_{13}	a_{14}	a_{15}	a_{16}	a_{17}	a_{18}	a_{19}
		a_{22}	a_{23}	a_{24}	a_{25}	a_{26}	a_{27}	a_{28}	a_{29}
			a_{33}	a_{34}	a_{35}	a_{36}	a_{37}	a_{38}	a_{39}
				a_{44}	a_{45}	a_{46}	a_{47}	a_{48}	a_{49}
					a_{55}	a_{56}	a_{57}	a_{58}	a_{59}
						a_{66}	a_{67}	a_{68}	a_{69}
							a_{77}	a_{78}	a_{79}
								a_{88}	a_{89}
									a_{99}

Fig. 1. Illustration of an attribute matrix for a route with $|R| = 10$.

as a fundamental component of our proposed tensor-based GPU acceleration method.

3.2 Sequence concatenation-based move evaluation

This section provides detailed calculations of the concatenation operations based on the attribute matrices. We focus on the most popular attributes, i.e., *travel distance*, *load related attributes*, and *time window related attributes*, which address the requirements of the studied VRPs (CVRP, VRPTW, VRP-SPDTW) and are widely used in vehicle routing. It is worth noting that concatenation operations can be similarly defined for other attributes found in other VRP variants, such as cumulative travel distance, load-dependent cost, and more, as discussed in [30].

3.2.1 Travel distance

Travel distance is the most important attribute in routing problems. Let σ be the node sequence or subsequence of a route and let $D(\sigma)$ be the travel distance of σ . For two route subsequences $\sigma_1 = \{v_i, \dots, v_j\}$ and $\sigma_2 = \{v_k, \dots, v_l\}$, let $\sigma_1 \oplus \sigma_2$ denote the concatenated sequence of σ_1 and σ_2 . Then the travel distance of the concatenated sequence $D(\sigma_1 \oplus \sigma_2)$ is computed as follows.

$$D(\sigma^0) = 0 \tag{2}$$

$$D(\sigma_1 \oplus \sigma_2) = D(\sigma_1) + c_{jk} + D(\sigma_2) \tag{3}$$

where σ^0 in Equation (2) denotes a subsequence containing a single node (whose distance is trivially 0) and c_{jk} in Equation (3) is the travel distance

between nodes j and k . Using the maintained travel distance attribute matrix, these computations can be done in constant time.

3.2.2 Load and capacity

To evaluate the load and capacity constraints, we need to track the load value before and after the sequence (L_i and L_o), as well as the maximum load (L_m). Additionally, we define the initial load values for a single node and establish the rules for concatenating two subsequences as follows. These computations can also be performed in constant time using the corresponding attribute matrices.

$$L_i(\sigma^0) = d_i, \quad L_o(\sigma^0) = p_i, \quad L_m(\sigma^0) = \max\{d_i, p_i\} \quad (4)$$

$$L_i(\sigma_1 \oplus \sigma_2) = L_i(\sigma_1) + L_i(\sigma_2) \quad (5)$$

$$L_o(\sigma_1 \oplus \sigma_2) = L_o(\sigma_1) + L_o(\sigma_2) \quad (6)$$

$$L_m(\sigma_1 \oplus \sigma_2) = \max\{L_m(\sigma_1) + L_i(\sigma_2), L_o(\sigma_1) + L_m(\sigma_2)\} \quad (7)$$

For the CVRP and the VRPTW, where the pickup demands are zero, the above formula remains valid. However, we can simplify the calculation by eliminating the pickup demand p_i and calculating only the maximum load L_m , resulting in the following expressions:

$$L_m(\sigma^0) = d_i \quad (8)$$

$$L_m(\sigma_1 \oplus \sigma_2) = L_m(\sigma_1) + L_m(\sigma_2) \quad (9)$$

3.2.3 Time windows

For the time window attribute, we use the time-warp technique [33,34] to manage the complexities associated with time window violations. For this, several other attributes are maintained for subsequences, including the earliest and latest arrival times (T_e and T_l), the duration time (T_d), and the value of any violated time window (T_v). Then the concatenation operation for the time window related attributes can be performed in constant time as follows.

$$T_d(\sigma^0) = s_i, \quad T_e(\sigma^0) = e_i, \quad T_l(\sigma^0) = l_i, \quad T_v(\sigma^0) = 0 \quad (10)$$

$$\Delta_t = T_d(\sigma_1) + T_w(\sigma_1) + t_{jk} - T_v(\sigma_1) \quad (11)$$

$$\Delta_w = \max\{T_e(\sigma_2) - \Delta_t - T_l(\sigma_1), 0\} \quad (12)$$

$$\Delta_v = \max\{T_e(\sigma_1) + \Delta_t - T_l(\sigma_2), 0\} \quad (13)$$

$$T_d(\sigma_1 \oplus \sigma_2) = T_d(\sigma_1) + t_{jk} + \Delta_w + T_d(\sigma_2) \quad (14)$$

$$T_e(\sigma_1 \oplus \sigma_2) = \max\{T_e(\sigma_1), T_e(\sigma_2) - \Delta_t\} - \Delta_w \quad (15)$$

$$T_l(\sigma_1 \oplus \sigma_2) = \min\{T_l(\sigma_1), T_l(\sigma_2) - \Delta_t\} + \Delta_v \quad (16)$$

$$T_v(\sigma_1 \oplus \sigma_2) = T_v(\sigma_1) + \Delta_v + T_v(\sigma_2) \quad (17)$$

In summary, by using different precomputed attribute matrices, we can efficiently compute the difference of attribute values between the original and modified solutions in constant time.

4 Tensor-based GPU acceleration for local search operators

In this section, we present the tensor-based GPU acceleration (TGA) method, which is designed to improve computational efficiency of commonly used local search operators in vehicle routing problems. The core of this method lies in the design of the tensor representation for solutions, which is based on the attribute matrices described in Section 3. By extracting and concatenating the relevant attribute tensors from the solution tensor representation, we can efficiently implement the sequence concatenation-based move evaluation with the help of GPU parallelism.

4.1 Workflow of the TGA method between CPU and GPU

The proposed TGA method is designed with a low degree of coupling between the CPU and the GPU. The computationally intensive evaluation of local search operators is entirely offloaded to the GPU. Meanwhile, the CPU handles only the updates based on the GPU's computation results. This design ensures that the TGA method can be easily integrated into a wide range of local search-based algorithms and frameworks. The workflow of the TGA method is illustrated in Figure 2.

The CPU initializes the solution tensor \mathbf{T}_s based on the given solution S and passes it to the GPU. On the GPU, local search operators are evaluated based on \mathbf{T}_s . To fully exploit the parallelism of the GPU, the best-improvement search strategy is used to select the best move among all possible moves. Once the best move is determined, it is sent back to the CPU, which updates

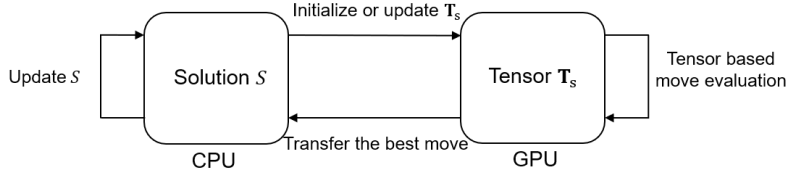


Fig. 2. Workflow of the TGA method.

the solution S . The updated solution tensor \mathbf{T}_s is then synchronized on the GPU. The rest of this section presents the details of the tensor representation and the implementation of the local search operators.

4.2 Attribute matrix-based tensor representation of routing solutions

As described in Section 3, we use several matrices to store precomputed solution attributes, which allows for constant-time move evaluation. Building on this, we combine these matrices into a solution tensor \mathbf{T}_s for GPU acceleration. Defined in Equation (18) and illustrated in Figure 3, \mathbf{T}_s is a 4-dimensional tensor with dimensions $I \times J \times K \times K$, where I is the number of maintained attributes, $J = M$ represents the number of routes, and $K = \max_{1 \leq i \leq M} \{|R_i|\}$ is the number of nodes in the longest route in terms of the number of nodes visited.

$$\mathbf{T}_s = (\mathbf{T}_s)_{ijkl} \in \mathbb{R}^{I \times J \times K \times K}, \quad i \in [1, I], j \in [1, J], k, l \in [1, K] \quad (18)$$

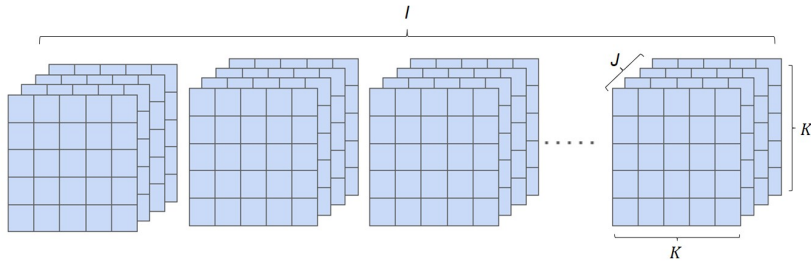


Fig. 3. Illustration of the solution tensor representation.

To handle travel distance and constraints related to time windows and capacity, we maintain the following key tensors of attributes: travel distance (\mathbf{D}), duration time (\mathbf{T}_d), earliest and latest arrival times (\mathbf{T}_e and \mathbf{T}_l), violated time window value (\mathbf{T}_v), load values before and after each subsequence (\mathbf{L}_i and \mathbf{L}_o), and maximum load (\mathbf{L}_m). To support efficient computation, auxiliary attributes are also stored: the first and last node indices of each sequence (\mathbf{I}_s

and \mathbf{I}_e) and a boolean mask (\mathbf{B}) indicating valid values. This attribute representation is customizable and can be extended to suit other VRP variants based on specific problem requirements.

4.3 Tensor-based local search operators

Using the solution tensor \mathbf{T}_s defined by Equation (18), we define the tensor-based implementation of the four common local search operators (*Relocate*, *Swap*, *2-opt**, and *2-opt*) in vehicle routing, taking advantage of GPU parallelism to speed up their evaluation process. The concatenation operations for these operators are illustrated in Figure 4. The *Relocate* operator moves a

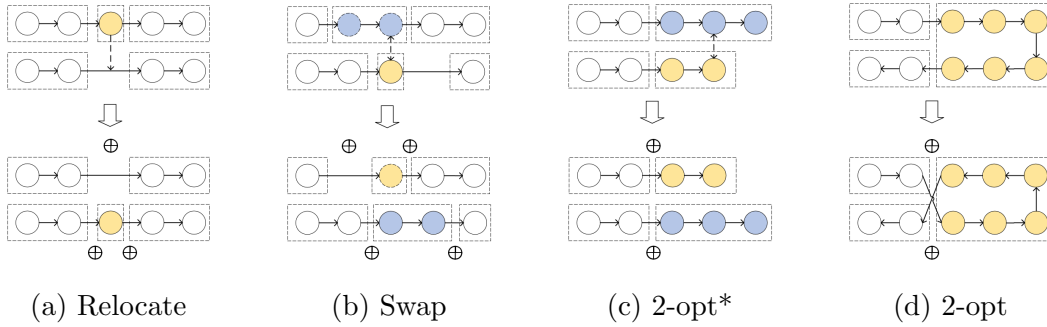


Fig. 4. Illustration of operators and concatenation operation

sequence of nodes to a new position within the same route or a different route, while the *Swap* operator exchanges two sequences of nodes. To clarify their implementations, these operations are categorized as *Intra-Relocate*, *Intra-Swap*, *Inter-Relocate*, and *Inter-Swap* depending on whether they operate within a single route or across two different routes. The *2-opt** operator, applied between two routes, breaks one edge in each route, exchanges the subsequences, and reconnects them to form new routes. In contrast, the *2-opt* move operates within a single route by breaking two non-adjacent edges and reconnecting the reversed subsequence. Note that *2-opt* is only suitable for problems with symmetric distance matrices and without directed constraints, such as time windows.

The tensor-based implementation for each operator follows a generic process composed of five steps: (1) Extract relevant parts of the solution tensor \mathbf{T}_s according to operators. (2) Compute attribute tensors representing all possible concatenated sequences within the operator’s neighborhood. (3) Compute the differences of attribute values between the original and modified routes. (4) Obtain the objective tensor \mathbf{F} based on the objective function and identify the best-improvement value and the corresponding indices in the objective tensor \mathbf{F} for the best move. (5) Update the solution S and the solution tensor \mathbf{T}_s based on the best move. The detailed description of these tensor-based

implementation steps is given below.

4.3.1 Extraction

The extraction step is crucial for distinguishing between different operators. Building on the concatenation operation for move evaluation outlined in Section 3, this step involves extracting specific parts of the solution tensor \mathbf{T}_s that represent the relevant subsequences of routes and contain all the corresponding attribute information needed to compute the attributes of the concatenated sequences in the subsequent steps.

Given the features of the tensor representation, we categorize the operators based on their application within the same route (referred to as intra-operators) or between two routes (referred to as inter-operators). Intra-operators include *Intra-Relocate*, *Intra-Swap*, and *2-opt*, while inter-operators consist of *Inter-Relocate*, *Inter-Swap*, and *2-opt**. This distinction allows for customized processing based on operator type.

$$\begin{aligned} \mathbf{S}_h &= (\mathbf{T}_s)_{::1l}, \quad l \in [1, K - 4] \\ \mathbf{S}_m &= (\mathbf{T}_s)_{::kl}, \quad k \in [2, K - 3], l \in [3, K - 2], \\ \mathbf{S}_t &= (\mathbf{T}_s)_{:jkl}, \quad j \in [1, J], k \in [4, K - 1], l = |R_j| \end{aligned} \quad (19)$$

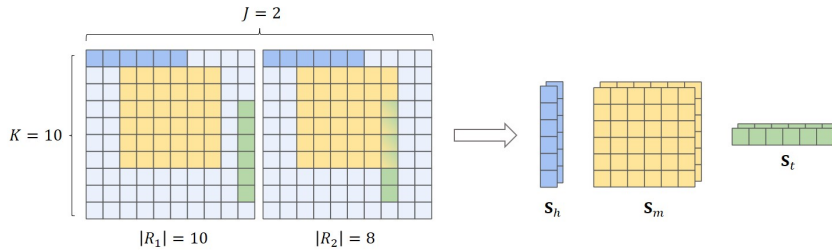


Fig. 5. An example of the extraction operation for *2-opt* and the reshape operation. We show a 3D tensor with dimensions $J \times K \times K = 2 \times 10 \times 10$, omitting the first dimension of \mathbf{T}_s .

Extraction for intra-operators: The intra-operators (*Intra-Relocate*, *Intra-Swap* and *2-opt*) involve only a single route, so we propose a route-based extraction for these operators. The *2-opt* operation divides the route into three subsequences: the head sequence \mathbf{S}_h , the middle sequence \mathbf{S}_m , and the tail sequence \mathbf{S}_t . The middle sequence contains the sequence to be reversed, the head sequence consists of the nodes preceding the middle sequence while the tail sequence includes the nodes following it. This extraction process can be described by Equation (19) and illustrated in Figure 5. Considering that the

2-opt operator is only applied to the variants with symmetric settings, the reverse of the middle sequence can be achieved by swapping the first and last node indices of the middle sequence. To ensure proper concatenation in the following steps, the extracted tensors must be appropriately reshaped. This reshaping process is applied consistently to all subsequent operators as well.

The *Intra-Relocate* operation divides the route into four subsequences: the head sequence S_h , the sequence to be relocated S_r , the destination sequence S_d , and the tail sequence S_t . There are two cases to consider based on the relative positions of S_r and S_d : either S_r precedes S_d or follows it. In both cases, the head and tail sequences remain unchanged. To optimize computational efficiency, we merge sequences S_r and S_d to address both cases simultaneously. The complete extraction process for *Intra-Relocate* is outlined in Equation (20). Figure 6 provides a visual example of the extraction process for the *Intra-Relocate* operator.

$$\begin{aligned}
\mathbf{S}_h &= (\mathbf{T}_s)_{::1l}, \quad l \in [1, K - N - 2] \\
\mathbf{S}_p &= \text{merge}(\mathbf{S}_r^1, \mathbf{S}_d^2) \\
\mathbf{S}_q &= \text{merge}(\mathbf{S}_d^1, \mathbf{S}_r^2) \\
\mathbf{S}_t &= (\mathbf{T}_s)_{:jkl}, \quad j \in [1, J], k \in [N + 3, K], l = |R_j| \\
\text{s.t. } \mathbf{S}_r^1 &= (\mathbf{T}_s)_{::k(k+N-1)}, \quad k \in [2, K - N - 1] \\
\mathbf{S}_d^2 &= (\mathbf{T}_s)_{::kl}, \quad k, l \in [2, K - N - 1] \\
\mathbf{S}_d^1 &= (\mathbf{T}_s)_{::kl}, \quad k, l \in [N + 2, K - 1] \\
\mathbf{S}_r^2 &= (\mathbf{T}_s)_{::k(k+N-1)}, \quad k \in [3, K - N]
\end{aligned} \tag{20}$$

Similarly, the *Intra-Swap* operation divides the routes into five subsequences:

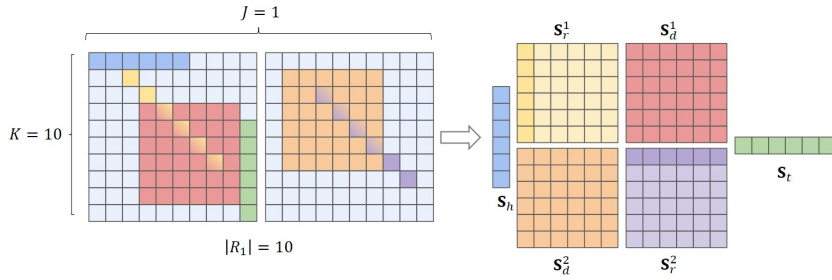


Fig. 6. An example of the extraction operation for *Intra-Relocate* with $N = 2$ and the reshape operation. We give only a 3D tensor with dimensions $J \times K \times K = 1 \times 10 \times 10$ to show its complicated extracted parts, omitting the first dimension of \mathbf{T}_s and setting $J = 1$.

the head sequence S_h , the sequence to be swapped S_p (of length N_1), the fixed sequence S_m , the second sequence to be swapped S_q (of length N_2), and the tail sequence S_t .

$$\begin{aligned}
& \mathbf{S}_h = (\mathbf{T}_s)_{::1l}, \quad l \in [1, K - N_1 - N_2 - 2] \\
& \mathbf{S}_p = \text{merge}(\mathbf{S}_r^1, \mathbf{S}_d^2) \\
& \mathbf{S}_m = \text{merge}(\mathbf{S}_m^1, \mathbf{S}_m^2) \\
& \mathbf{S}_q = \text{merge}(\mathbf{S}_d^1, \mathbf{S}_r^2) \\
& \mathbf{S}_t = (\mathbf{T}_s)_{:jkl}, \quad j \in [1, J], k \in [N_1 + N_2 + 3, K], l = |R_j| \\
\text{s.t.} \quad & \mathbf{S}_r^1 = (\mathbf{T}_s)_{::k(k+N_1-1)}, \quad k \in [2, K - N_1 - N_2 - 1] \\
& \mathbf{S}_d^2 = (\mathbf{T}_s)_{::k(k+N_2-1)}, \quad k \in [2, K - N_1 - N_2 - 1] \\
& \mathbf{S}_m^1 = (\mathbf{T}_s)_{::kl}, \quad k, l \in [N_1 + 2, K - N_2 - 1] \\
& \mathbf{S}_m^2 = (\mathbf{T}_s)_{::kl}, \quad k, l \in [N_2 + 2, K - N_1 - 1] \\
& \mathbf{S}_d^1 = (\mathbf{T}_s)_{::k(k+N_2-1)}, \quad k \in [N_1 + 3, K - N_2] \\
& \mathbf{S}_r^2 = (\mathbf{T}_s)_{::k(k+N_1-1)}, \quad k \in [N_2 + 3, K - N_1]
\end{aligned} \tag{21}$$

When the lengths of the two sequences differ, there are two cases to consider. A merging process is also applied to optimize the extraction. The complete extraction process for *Intra-Swap* is detailed in Equation (21). Figure 7 illus-

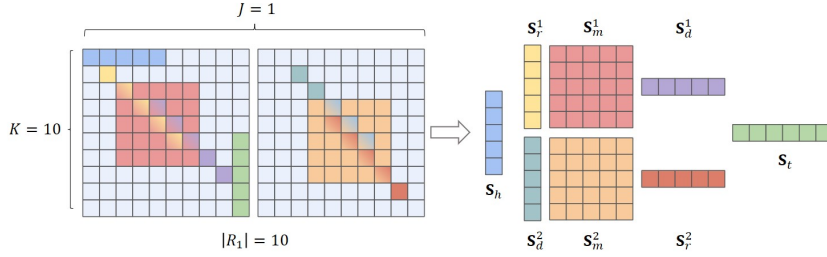


Fig. 7. An example of the extraction operation for *Intra-Swap* with $N_1 = 1, N_2 = 2$ and the reshape operation. We give only a 3D tensor with dimensions $J \times K \times K = 1 \times 10 \times 10$ to show its complicated extracted parts, omitting the first dimension of \mathbf{T}_s and setting $J = 1$.

trates the extraction process for the *Intra-Swap* operator.

Extraction for inter-operators: Building on the same principle used for intra-operators, we extend the route-based extraction approach to inter-operators (*Inter-Relocate*, *Inter-Swap*, and *2-opt**). These operators share a similar schema, implemented using the so-called 3-Seq operation. That is, we split the routes into a head sequence \mathbf{S}_h , a middle sequence \mathbf{S}_m , and a tail sequence \mathbf{S}_t , while its middle sequence \mathbf{S}_m represents the sequence to be relocated or swapped. The route-based 3-Seq(N) operation is described by Equation (22), where N represents the length of the sequence to be relocated or swapped. Note that the middle sequence \mathbf{S}_m is empty when $N = 0$, which occurs in the *2-opt** and *Inter-Relocate* operators. Figure 8 illustrates the route-based implementation of the 3-Seq operation.

$$\begin{aligned}
\mathbf{S}_h &= (\mathbf{T}_s)_{::1l}, \quad l \in [1, K - N - 1], N \geq 0 \\
\mathbf{S}_m &= (\mathbf{T}_s)_{::k(k+N-1)} \text{ for } N > 0, k \in [2, K - N]; \emptyset \text{ for } N = 0. \\
\mathbf{S}_t &= (\mathbf{T}_s)_{:jkl}, \quad j \in [1, J], k \in [N + 2, K], l = |R_j|, N \geq 0
\end{aligned} \tag{22}$$

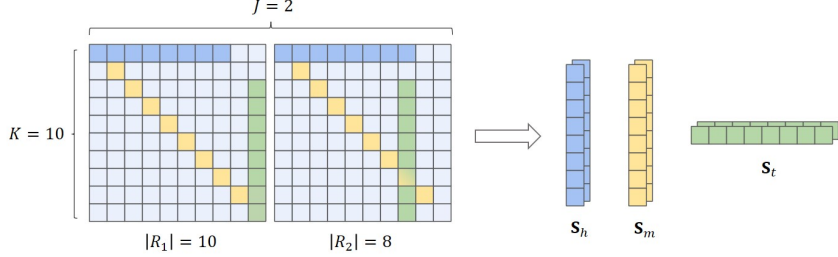


Fig. 8. An example of the route-based implementation of 3-Seq operation with $N = 1$ for inter-operators and reshape operation. Here we show a 3D tensor with dimensions $J \times K \times K = 2 \times 10 \times 10$, omitting the first dimension of \mathbf{T}_s for clarity. Note that the length of the routes affects the tail sequence \mathbf{S}_t .

It is worth noting that the route-based implementation of the 3-Seq operation can result in high-dimensional intermediate and objective tensors, along with increased computational complexity in subsequent steps, because the inter-operators involves the computation between routes. A detailed complexity analysis is provided in Section 4.4. To address these challenges, we propose a more efficient alternative: the node-based implementation of the 3-Seq operation. In this approach, we first extract the positional information $\mathbf{P} = [\mathbf{R}, \mathbf{I}]$ from the solution tensor \mathbf{T}_s , where \mathbf{R} indicates the route index of each valid node (including depot nodes and customer nodes), and \mathbf{I} denotes the node's position within its route. Using this positional information, we then extract the head sequence \mathbf{S}_h , the middle sequence \mathbf{S}_m , and the tail sequence \mathbf{S}_t for all valid nodes. The node-based implementation is formalized in Equation (23), and an illustrative example is shown in Figure 9. The key distinction between the two implementations is that the route-based method extracts subsequences based on the route structure, which may include invalid elements due to the maximum route length value K , whereas the node-based method focuses on valid nodes using positional information, resulting in greater computational efficiency.

Using the 3-Seq operation, we can accurately define the extraction process for the inter-operators. The *Inter-Relocate* operator involves a 3-Seq(N) ($N > 0$) operation and a 3-Seq(0) operation. The *Inter-Swap* operator requires two separate operations: 3-Seq(N_1) and 3-Seq(N_2) ($N_1, N_2 > 0$). The *2-opt** operator relies solely on 3-Seq(0) operations.

To summarize, in the standard implementation of TGA, intra-operators use route-based extraction, while inter-operators adopt the node-based implementation of the 3-Seq operation.

$$\begin{aligned}
\mathbf{S}_h &= (\mathbf{T}_s)_{:\mathbf{R}1(\mathbf{I}-1)}, \text{ for } N > 0; (\mathbf{T}_s)_{:\mathbf{R}1\mathbf{I}} \text{ for } N = 0. \\
\mathbf{S}_m &= (\mathbf{T}_s)_{:\mathbf{R}1(\mathbf{I}+N-1)} \text{ for } N > 0; \emptyset \text{ for } N = 0. \\
\mathbf{S}_t &= (\mathbf{T}_s)_{:\mathbf{R}(\mathbf{I}+N)\mathbf{L}_R}, \text{ for } N > 0; (\mathbf{T}_s)_{:\mathbf{R}(\mathbf{I}+1)\mathbf{L}_R} \text{ for } N = 0, \mathbf{L} = \{|R_i|, |R_2|, \dots, |R_J|\}.
\end{aligned} \tag{23}$$

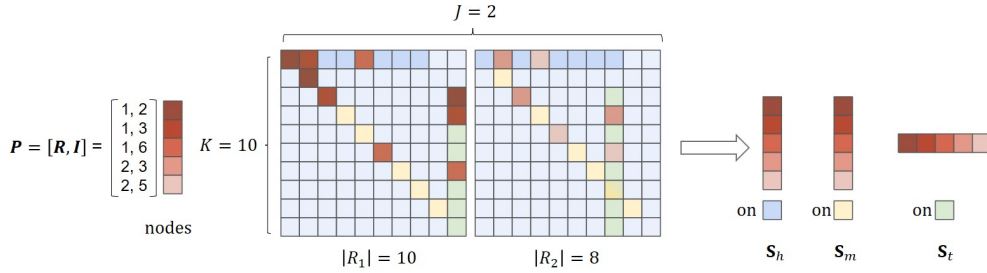


Fig. 9. An example of the node-based implementation of the 3-Seq operation. To illustrate the differences between node-based and route-based implementations, we reuse the same setting as in Figure 8. In this example, five nodes are distributed across two routes: the 2nd, 3rd, and 6th nodes on route R_1 , and the 3rd and 5th nodes on route R_2 . The figure shows how the head, middle, and tail sequences are extracted based on node positions, and highlights their relationship to those obtained through the route-based method.

4.3.2 Concatenation

This section outlines the concatenation operation for two sequences of nodes, using the tensors extracted in the previous section. The extracted tensors need to be sliced along the first dimension to obtain the attribute tensors. The concatenation operation is then applied to these attribute tensors to compute the attributes of the concatenated sequences.

$$\mathbf{D}(\sigma_1 \oplus \sigma_2) = \mathbf{D}(\sigma_1) + \mathbf{C}[\mathbf{I}_e(\sigma_1), \mathbf{I}_s(\sigma_2)] + \mathbf{D}(\sigma_2) \tag{24}$$

$$\mathbf{T}_d(\sigma_1 \oplus \sigma_2) = \mathbf{T}_d(\sigma_1) + \mathbf{T}[\mathbf{I}_e(\sigma_1), \mathbf{I}_s(\sigma_2)] + \mathbf{T}_d(\sigma_2) \tag{25}$$

Most attributes can be calculated directly using the formulas for concatenation operations as described in Section 3.2, allowing efficient parallelization on the GPUs. However, the computation of travel distance and duration time must take into account additional travel and time costs when connecting two

sequences of nodes. These values can be derived from the travel distance tensor \mathbf{C} , the travel time tensor \mathbf{T} , and the first node index tensor \mathbf{I}_s and the last node index tensor \mathbf{I}_e of the sequences. The specific concatenation processes for travel distance \mathbf{D} and duration time \mathbf{T}_d are described in Equations (24) and (25).

4.3.3 Difference

To calculate the objective function's variation, we compute the differences in key attributes between the original and modified routes. The attributes of the original route are stored in the tensor \mathbf{T}_s , while the attributes of the modified routes are obtained by concatenation. This enables straightforward computation of the difference values, such as the travel distance $\Delta\mathbf{D}$, the violated time window value $\Delta\mathbf{T}_v$, and the violated load value $\Delta\mathbf{L}_v$.

4.3.4 Objective

Using the difference values calculated in the previous step, we can compute the delta objective value tensor \mathbf{F} based on the defined objective or evaluation function \mathcal{F} , as shown in Equation (26). Note that some values in the objective tensor \mathbf{F} are invalid. To address this, we use the boolean mask tensor \mathbf{B} to filter out these invalid values by assigning a very large value to them as shown in Equation (27).

$$\mathbf{F} = \mathcal{F}(\Delta\mathbf{D}, \Delta\mathbf{T}_v, \Delta\mathbf{L}_v) \quad (26)$$

$$\mathbf{F} \leftarrow \mathbf{F} + (\neg\mathbf{B}) \cdot \infty \quad (27)$$

$$F_{\min} = \mathbf{F}_{\alpha^*} \quad \text{where} \quad \alpha^* = \arg \min_{\alpha} \mathbf{F}_{\alpha} \quad (28)$$

Next, we extract the minimal objective value and its corresponding indices from the objective tensor \mathbf{F} using Equation (28). The resulting indices α^* encode the information necessary to identify the best move, including the involved routes and the starting positions of the sequences to be relocated or swapped. Finally, the best move information is sent to the CPU to update the solution and the tensor representation \mathbf{T}_s .

4.3.5 Tensor update

Once the chosen best move is performed on the CPU, the solution tensor representation \mathbf{T}_s needs to be updated based on the new resulting solution. Since the operators considered only impact one or two routes, it is unnecessary to update the entire tensor \mathbf{T}_s . Instead, only the affected parts need to be

modified. The update process consists of two main steps: (1) Resize the tensor \mathbf{T}_s if any routes are removed or if the longest route length K changes. (2) Update the attribute values of the affected routes on the tensor representation \mathbf{T}_s on GPU.

4.4 Complexity analysis

In this section, we analyze the complexity of the tensor-based GPU acceleration method, assuming the GPU can launch p threads in parallel.

For the initialization, the solution tensor representation \mathbf{T}_s with dimensions $I \times J \times K \times K$ is constructed, where I is the number of attributes, J is the number of routes, and K is the maximum route length. This setup results in a space complexity of $O(I \cdot J \cdot K^2)$ and a time complexity of $O(\frac{I \cdot J \cdot K^2}{p})$. The tensor update involves modifying the affected part of the tensor representation \mathbf{T}_s based on the best move, which has a space complexity of $O(I \cdot K^2)$ and a time complexity of $O(\frac{I \cdot K^2}{p})$. Note that the time complexity approaches $O(1)$ with maximum parallelism (very large p).

For the execution of the local search operators, we analyze the complexity for each step as follows.

The Extraction step involves slicing and reshaping the solution tensor \mathbf{T}_s to obtain the relevant attributes of subsequences. The worst-case complexity for creating the extracted tensors is determined by the shape of the extracted tensors. The inter-operators, which are based on the node-based implementation of 3-Seq operation, have a space complexity of $O(I \cdot (\mathcal{N} + J))$ and a time complexity of $O(\frac{I \cdot (\mathcal{N} + J)}{p})$, where $\mathcal{N} + J$ represents the number of customers and vehicles. The intra-operators have a space complexity of $O(I \cdot J \cdot (K - N)^2)$ and a time complexity of $O(\frac{I \cdot J \cdot (K - N)^2}{p})$. In an ideal case, these operations can also reach $O(1)$.

In the Concatenation step, new attribute tensors are computed for the concatenated sequences. The space complexity is $O(I \cdot (\mathcal{N} + J)^2)$ for the inter-operators and $O(I \cdot J \cdot (K - N)^2)$ for the intra-operators. Since the attributes calculated respectively according to specific formulas, the time complexity is $O(I \cdot \frac{(\mathcal{N} + J)^2}{p})$ for the inter-operators and $O(I \cdot \frac{J \cdot (K - N)^2}{p})$ for intra-operators. Under ideal parallelism, the time complexity can be reduced to $O(I)$.

The Difference step only computes delta tensors for specific attributes based on the objective requirements. For the inter-operators, the complexity is $O((\mathcal{N} + J)^2)$ in space and $O(\frac{(\mathcal{N} + J)^2}{p})$ in time. For the intra-operators, the complexity is $O(J \cdot (K - N)^2)$ in space and $O(\frac{J \cdot (K - N)^2}{p})$ in time. The ideal time complexity

remains $O(1)$.

The Objective step has the same space complexity as the Difference step, as the final objective tensor \mathbf{F} is computed from the delta tensors. Unlike other operations, identifying the best move involves a reduction operation, which has a time complexity of $O(\frac{n}{p} + \log(p))$ for a tensor with n elements and p threads. This complexity arises because each thread initially reduces $\frac{n}{p}$ elements in parallel, and then the partial results are further combined across $\log(p)$ steps. Thus, Objective step yields a time complexity of $O(\frac{(\mathcal{N}+J)^2}{p} + \log(p))$ for the inter-operators and $O(\frac{J \cdot (K-N)^2}{p} + \log(p))$ for the intra-operators. In an ideal parallel case, these complexities can reduce to $O(\log((\mathcal{N} + J)^2))$ and $O(\log(J \cdot (K - N)^2))$, respectively.

In summary, for the inter-operators, the total space complexity is $O(I \cdot (\mathcal{N} + J)^2)$, and the time complexity is $O(\frac{I \cdot (\mathcal{N}+J)}{p} + I \cdot \frac{(\mathcal{N}+J)^2}{p} + \frac{(\mathcal{N}+J)^2}{p} + \log(p))$. For the intra-operators, the total space complexity is $O(I \cdot J \cdot (K - N)^2)$, and the time complexity is $O(\frac{I \cdot J \cdot (K-N)^2}{p} + I \cdot \frac{J \cdot (K-N)^2}{p} + \frac{J \cdot (K-N)^2}{p} + \log(p))$. In an ideal scenario with maximum parallelism, the time complexities reduce to $O(I + \log((\mathcal{N} + J)^2))$ and $O(I + \log(J \cdot (K - N)^2))$, respectively.

Additionally, for the inter-operators based on route-based 3-Seq operation, the total space complexity is $O(I \cdot J^2 \cdot (K - N)^2)$, where $K - N$ is the effective subsequence length. The corresponding time complexity is $O(\frac{I \cdot J \cdot (K-N)}{p} + I \cdot \frac{J^2 \cdot (K-N)^2}{p} + \frac{J^2 \cdot (K-N)^2}{p} + \log(p))$. In the ideal case, the time complexity can be reduced to $O(I + \log(J^2 \cdot (K - N)^2))$. It is evident that the route-based implementation has higher complexity in both space and time compared to the node-based implementation, due to high dimensional intermediate and objective tensors containing the invalid entries.

Through analysis, it becomes clear that the overall time complexity depends heavily on the size of the objective tensor \mathbf{F} . When \mathbf{F} is large, the Objective step dominates the computational cost. Otherwise, the computational cost is mainly influenced by the other steps, with the Concatenation step being particularly significant.

5 Computational results

This section presents computational experiments to evaluate the performance of the proposed tensor-based GPU acceleration for common local search operators in vehicle routing problems.

It is important to note that the goal of this study is not to set new records

for the benchmark instances. Instead, the goal is to explore the potential of the proposed TGA method for solving vehicle routing problems and to provide a foundation for future research in this direction. Accordingly, the following sections focus on designing fair and consistent experiments to assess the effectiveness of the TGA method, particularly in terms of computational efficiency, compared to traditional CPU-based implementations.

5.1 Algorithms for experimentation

This section provides a detailed overview of the algorithms used in the comparative study to evaluate the performance of the proposed tensor-based GPU acceleration method.

Our tensor-based GPU acceleration (TGA) method is highly extensible and can be integrated into various local search based algorithms and frameworks. To demonstrate its performance, we incorporated TGA into the MA-FIRD algorithm [32], which has shown its effectiveness in solving the VRPSPDTW. Since the CVRP and the VRPTW are special cases of the VRPSPDTW, this integration allows the algorithm to address these variants as well, even though the original MA-FIRD algorithm was not specifically designed for solving the CVRP or VRPTW.

MA-FIRD [32] is a memetic algorithm that combines a feasible and infeasible route descent search (FIRD) and an adaptive route-inheritance crossover (ARIX). The FIRD is a local search procedure using the best-improvement strategy and the sequence concatenation-based move evaluation method. The ARIX crossover generates offspring solutions by inheriting routes from multiple parent solutions and incorporates a learning mechanism to adaptively adjust the number of parents and the heuristics used to complete the partial offspring under construction.

To evaluate the performance of TGA, we modified the initial MA-FIRD algorithm of [32] and incorporated TGA, and we use MA-TGA to denote the resulting TGA-based algorithm. The overall MA-TGA algorithm is shown in Algorithm 1. For a given problem instance \mathcal{I} , the algorithm begins by generating an initial population \mathcal{P} consisting of $N_{\mathcal{P}}$ candidate solutions (line 4), with the best solution S^* being recorded (line 5). The algorithm then iteratively updates the population by creating new candidate solutions (lines 6-18). In each generation, the adaptive route-inheritance crossover (ARIX) generates a new solution S (line 7), which is then improved using feasible and infeasible search based on the given local search operators in \mathcal{O} , with the implementation of our proposed TGA method (line 8). Note that the route descent strategy is omitted in this setting to simplify the search process and ensure compatibility

with problem variants that do not consider the number of vehicles as an objective. The improved solution S is used to update the population according to the population management strategy (line 9). If an improved best solution is found, S^* is updated, and the stagnation counter is reset to zero (lines 11-13). Otherwise, the stagnation generation counter φ_{st} increments (lines 14-15). The algorithm terminates and returns the best solution S^* (line 19) when a termination condition is reached (line 6).

Algorithm 1 General framework of MA-TGA

```

1: Input: Instance  $\mathcal{I}$ , population size  $\mathcal{N}_{\mathcal{P}}$ , maximum number of generations
    $\varphi_{max}$ , patience for stagnation generations  $\rho$ , maximum running time  $\tau$ , set
   of operators  $\mathcal{O} = \{O_1, O_2, \dots, O_n\}$ .
2: Output: The best solution  $S^*$ .
3:  $\varphi \leftarrow 0, \varphi_{st} \leftarrow 0$  /* Current generation and stagnation generation counter
   */
4:  $\mathcal{P} \leftarrow Initialization(\mathcal{I}, \mathcal{N}_{\mathcal{P}})$ 
5:  $S^* \leftarrow BestSolution(\mathcal{P})$  /* Record current best solution */
6: while  $\varphi \leq \varphi_{max}$  and  $\varphi_{st} \leq \rho$  and  $time() \leq \tau$  do
7:    $S \leftarrow ARIX(\mathcal{P})$ 
8:    $S \leftarrow FeasibleInfeasibleSearch(S, \mathcal{O})$ 
9:    $\mathcal{P} \leftarrow UpdatePopulation(S, \mathcal{P})$ 
10:   $S_{best} \leftarrow BestSolution(\mathcal{P})$  /* The best solution in this generation */
11:  if  $f(S_{best}) < f(S^*)$  then
12:     $S^* \leftarrow S_{best}$  /* Update the best solution */
13:     $\varphi_{st} \leftarrow 0$ 
14:  else
15:     $\varphi_{st} \leftarrow \varphi_{st} + 1$  /* Stagnation counter is incremented */
16:  end if
17:   $\varphi = \varphi + 1$ 
18: end while
19: return  $S^*$ 

```

In MA-TGA, the TGA-based feasible and infeasible search (Algorithm 2) is the key local search component ensuring the role of search intensification. It exploits *Relocate*, *Swap*, and *2-opt** for the VRPTW and the VRPSPDTW, plus *2-opt* for the CVRP.

For the purpose of our comparative study, we adopt the CPU-only version (denoted as MA) using the traditional implementation of the above local search operators. Specifically, in MA, the local search procedure excludes lines 3 and 9 of Algorithm 2 and uses the traditional CPU processing for the evaluation in line 6.

To enable a clear and unbiased analysis of the speedup performance introduced by TGA, both MA and MA-TGA adopt the same best-improvement local search strategy without any additional neighborhood reduction or prun-

Algorithm 2 Feasible and infeasible search of MA-TGA

```
1: Input: Input solution  $S$ , set of operators  $\mathcal{O} = \{O_1, O_2, \dots, O_n\}$ .
2: Output: Improved solution  $S$ .
3: Initialize tensor  $\mathbf{T}_s$  on GPU based on the solution  $S$ .
4: while The given termination criterion is not met do
5:   Select an operator  $O_i \in \mathcal{O}$ .
6:    $\zeta \leftarrow Evaluate(\mathbf{T}_s, S, O_i)$  /*Evaluate the neighborhood of the operator
    $O_i$  and obtain the best move  $\zeta^*$ /.
7:   if The move  $\zeta$  is accepted based on the defined evaluation then
8:     Update current solution  $S$  based on the move  $\zeta$ .
9:     Update tensor  $\mathbf{T}_s$  based on current solution  $S$ .
10:  end if
11: end while
12: return  $S$ 
```

ing techniques. While such techniques are widely used in the literature to improve the efficiency of local search algorithms, they are excluded in this study to ensure a fair and controlled comparison between the two algorithms. This setup allows us to isolate the contribution of TGA to the computational performance, even though excluding these enhancements may significantly affect the overall solution quality or efficiency.

In summary, both MA and MA-TGA share the same algorithmic framework, with the main difference that MA uses the traditional evaluation methods for the local search operators, while MA-TGA uses the proposed tensor-based GPU acceleration method.

5.2 Benchmark instances

We assess the proposed method on three VRP variants: the capacitated VRP (CVRP), VRP with time windows (VRPTW), and the VRP with simultaneous pickup and delivery and time windows (VRPSPDTW), using widely recognized benchmark instances from the literature.

For the CVRP, we use the X benchmark from [35], which includes 100 instances with sizes ranging from 100 to 1000. For the VRPTW, we rely on the GH instances from [36], comprising 300 instances with 200 to 1000 customers, divided into three types: C (clustered customers), R (randomly distributed customers), and RC (a mix of clustered and random). Each of these types includes instances with narrow time windows and small vehicle capacities, as well as instances with wide time windows and larger vehicle capacities. For the VRPSPDTW, we employ the JD benchmark from [31], based on real-world data from JD Logistics, with 20 instances across customer sizes of 200, 400,

600, 800, and 1000.

We conducted experiments on a representative subset of 50 instances: 10 X instances for CVRP, 30 GH instances for VRPTW, and 10 JD instances for VRPSPDTW, covering a diverse range of different instance sizes and types for comprehensive analysis.

5.3 Experimental protocol

Both the MA and MA-TGA algorithms are implemented in C++, with the tensor-based GPU acceleration in MA-TGA utilizing the PyTorch C++ API. The source codes of both algorithms will be publicly available when the paper is published. Experiments were conducted on an Intel Xeon E5-2690 v4 2.60 GHz processor and an NVIDIA A40 GPU with 48 GB memory.

We kept the parameter settings from MA-FIRD [32], with the population size $\mathcal{N}_p = 10$, the maximum generations $\varphi_{max} = 5000$, the patience threshold for stagnation $\rho = 500$, the fitness function coefficient $\xi = 0.8$, the adjustment factor $\kappa = 0.5$, and the initial retention ratio $\gamma_r^0 = 0.9$. The time limit τ is set to 3600 seconds for X (CVRP) instances, 7200 seconds for GH (VRPTW) and JD (VRPSPDTW) instances. Each instance was solved five times by each algorithm.

5.4 Computational results and comparisons

Table 1 presents a comparative summary of MA-TGA and MA across 50 benchmark instances. The *#Instance* column indicates the number of tested instances within each benchmark set. The *#Win*, *#Tie*, and *#Loss* columns report the number of instances where MA-TGA performs better, equal, or worse compared to MA in terms of the best result among 5 runs. Statistical significance is assessed using the Wilcoxon signed-rank test [37], with results reported in the *p-value* column at a 0.05 significance level. The results show that MA-TGA outperformed MA on 31 instances (62%) and matched performance on 13 instances (26%), with statistically significant differences (*p-values* $\ll 0.05$).

Tables 2-4 present the average results from 5 runs on the X (CVRP), GH (VRPTW), and JD (VRPSPDTW) benchmarks. Columns include instance name (*Instance*), size or number of customers (\mathcal{N}), number of vehicles (M), objective value (f), and running time (t). Gap(%) shows the percentage improvement of MA-TGA over MA in objective value, where a negative gap indicates better performance.

Table 1

Summary of comparative results between MA-TGA and MA on three benchmark instances.

Benchmark	#Instance	#Win	#Tie	#Loss	<i>p-value</i>
<i>X</i>	10	7	1	2	8.86E-05
<i>GH</i>	30	14	12	4	2.30E-26
<i>JD</i>	10	10	0	0	1.78E-15
Total	50	31	13	6	-

Table 2

Average comparative results on the 10 *X* benchmark instances of the CVRP between MA and MA-TGA.

Instance	\mathcal{N}	MA (Avg)			MA-TGA (Avg)			
		<i>M</i>	<i>f</i>	<i>t</i>	<i>M</i>	<i>f</i>	<i>t</i>	Gap(%)
X-n101-k25	100	26.0	27646.00	76.60	26.0	27606.20	192.89	-0.14
X-n200-k36	199	36.0	58804.60	500.46	36.0	58802.20	538.68	0.00
X-n303-k21	302	21.0	22055.40	1632.04	21.0	22032.40	306.30	-0.10
X-n401-k29	400	29.0	66794.40	1811.85	29.0	66741.40	525.07	-0.08
X-n502-k39	501	39.0	69709.80	1219.43	39.0	69715.20	420.64	0.01
X-n627-k43	626	43.2	63963.40	3601.54	43.0	63374.80	837.57	-0.92
X-n701-k44	700	44.0	83907.60	3601.72	44.0	84009.00	1030.34	0.12
X-n801-k40	800	40.0	75322.40	3600.51	40.0	74805.40	1381.17	-0.69
X-n916-k207	915	208.8	344134.60	3621.72	207.6332869.80	3600.77		-3.27
X-n1001-k43	1000	43.0	76357.20	3605.59	43.0	74510.00	2887.74	-2.42
MEAN	-	53.0	88869.54	2327.15	52.9	87446.64	1172.11	-0.75

The TGA method demonstrates significant performance improvements (better results) and computational efficiency gains on most benchmark instances, especially for large-scale instances. Compared to the traditional CPU-based MA method, MA-TGA achieves better average results with average improvements (gaps) of -0.75%, -0.93%, and -1.82% for the *X*, *GH*, and *JD* instances, respectively. These gains are generally achieved within shorter computational times for instances with more than 200 nodes, demonstrating the computation efficiency and improved search capacity of the TGA method compared to MA with traditional CPU-based implementations.

5.5 Analysis of overall speedup ratio

To gain an intuitive understanding of the overall speedup achieved by MA-TGA over MA, we conducted additional experiments to analyze the speedup ratios across benchmark instances. Let t_{MA} denote the total runtime of MA based on CPU implementation after 100 iterations, and $t_{\text{MA-TGA}}$ the runtime

Table 3

Average comparative results on the 30 *GH* benchmark instances of the VRPTW between MA and MA-TGA.

Instance	\mathcal{N}	MA (Avg)			MA-TGA (Avg)			
		M	f	t	M	f	t	Gap(%)
C1.2.1	200	20.0	2698.60	81.85	20.0	2698.60	53.75	0.00
C2.2.1	200	7.0	1922.10	59.95	7.0	1922.10	37.02	0.00
R1.2.1	200	23.0	4667.20	621.62	22.8	4669.20	388.11	0.04
R2.2.1	200	9.6	3543.22	267.36	8.6	3604.06	197.88	1.72
RC1.2.1	200	20.0	3518.44	813.90	20.0	3517.92	713.47	-0.01
RC2.2.1	200	9.0	2801.72	168.19	9.0	2799.08	104.05	-0.09
C1.4.1	400	40.0	7138.80	597.16	40.0	7138.80	99.47	0.00
C2.4.1	400	12.0	4100.30	488.78	12.0	4100.30	64.71	0.00
R1.4.1	400	41.2	10352.00	6625.91	41.010336.76	1223.88		-0.15
R2.4.1	400	15.8	7773.04	2166.92	16.2	7741.28	257.78	-0.41
RC1.4.1	400	37.0	8564.68	6702.30	37.0	8560.72	1152.49	-0.05
RC2.4.1	400	16.4	6169.84	2604.35	16.0	6171.50	563.60	0.03
C1.6.1	600	60.0	14076.60	1987.89	60.014076.60	118.71		0.00
C2.6.1	600	18.4	7763.60	1737.44	18.0	7753.40	80.48	-0.13
R1.6.1	600	59.8	21711.38	7228.67	58.221385.04	2558.17		-1.50
R2.6.1	600	22.0	15531.76	7201.83	23.015433.28	480.66		-0.63
RC1.6.1	600	56.6	17338.40	7207.39	56.817120.64	2872.24		-1.26
RC2.6.1	600	22.2	12033.08	7205.75	21.412054.24	461.22		0.18
C1.8.1	800	80.0	25156.90	5125.81	80.025156.90	211.37		0.00
C2.8.1	800	24.0	11632.74	6046.53	24.011632.90	194.65		0.00
R1.8.1	800	81.8	37422.26	7253.38	79.836803.78	2370.07		-1.65
R2.8.1	800	23.6	26213.94	7221.89	25.825399.82	1172.64		-3.11
RC1.8.1	800	75.4	31006.96	7284.23	74.030213.52	5260.46		-2.56
RC2.8.1	800	26.0	19624.10	7214.62	25.619285.50	767.04		-1.73
C1.10.1	1000	100.0	42444.98	7209.73	100.042444.80	502.18		0.00
C2.10.1	1000	30.0	16841.10	5194.01	30.016841.10	148.01		0.00
R1.10.1	1000	99.4	55227.10	7337.51	94.653696.60	4856.53		-2.77
R2.10.1	1000	26.2	40171.88	7240.21	33.437356.76	1624.20		-7.01
RC1.10.1	1000	93.0	47832.22	7288.73	91.246635.00	6435.92		-2.50
RC2.10.1	1000	28.4	29635.00	7268.74	29.428379.20	2335.93		-4.24
MEAN	-	39.3	17830.46	4515.09	39.217497.65	1243.56		-0.93

of the corresponding TGA implementation over the same number of iterations. The speedup ratio is then defined as $\gamma_s = \frac{t_{MA}}{t_{MA-TGA}}$. Each instance is executed five times, and both MA and MA-TGA follow the same search trajectories in each run to guarantee fair and consistent comparisons. Figure 10 visualizes the speedup ratio across the tested instances, illustrating the relationship between

Table 4

Average comparative results on the 10 *JD* benchmark instances of the VRPSPDTW between MA and MA-TGA.

Instance	\mathcal{N}	MA (Avg)			MA-TGA (Avg)			
		M	f	t	M	f	t	Gap(%)
F201	200	40.8	64754.08	720.98	41.0	64821.06	402.34	0.10
F203	200	41.2	65898.84	745.34	41.0	65867.50	594.34	-0.05
F401	400	76.8	117813.40	7005.46	76.4117611.80		1011.34	-0.17
F403	400	77.0	117523.60	3918.32	76.6117189.80		782.19	-0.28
F601	600	112.4	176693.00	7201.35	110.4174765.00		1575.29	-1.09
F603	600	114.4	180993.80	7202.04	113.6178970.80		1481.39	-1.12
F801	800	156.8	216575.80	7206.97	148.8208419.80		2887.08	-3.77
F803	800	156.8	215511.80	7212.35	151.2209893.80		2867.29	-2.61
F1001	1000	203.8	312252.60	7366.01	192.6298006.80		6082.87	-4.56
F1003	1000	204.2	310444.60	7298.24	194.0295922.80		5526.28	-4.68
MEAN	-	118.4	177846.15	5587.71	114.6173146.92		2321.04	-1.82

instance size and speedup ratio for different benchmark instances.

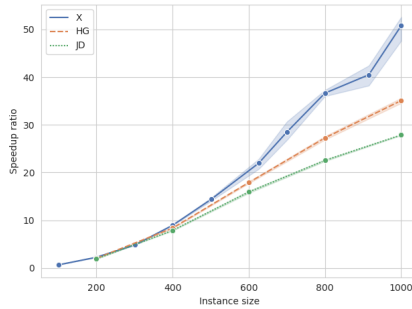


Fig. 10. Correlations between instance size and speedup ratio across different benchmark instances. The x-axis represents instance size and the y-axis shows MA-TGA speedup ratio over MA. The lines indicate the mean relative speedup for each benchmark and the shaded areas represent the 0.95 confidence interval.

The results demonstrate a clear positive correlation between instance size and speedup ratio for the *GH* (VRPTW) and *JD* (VRPSPDTW) benchmarks. As the instance size increases from 200 to 1000 nodes, the speedup ratio increases from about 2 to nearly 30, which is in line with theoretical expectations and highlights the computational gains offered by TGA for larger instances.

A similar trend is observed for the *X* (CVRP) instances, with even higher speedup ratios on larger instances due to the less constrained nature of CVRP. For example, the 1000-node instance achieves a speedup of nearly 50 times. Note that on small instances with 100 nodes, the acceleration effect of TGA is not observed. This is because these instances are relatively small and computationally simple, making the overhead of GPU operation outweigh the performance gains. This observation highlights the particular interest of the

proposed TGA method for handling challenging and large scale instances.

In addition, some variability is observed in the speedup curve for the X (CVRP) instances due to different characteristics of the instances tested, especially the number of vehicles required. For example, the 800-node instance requires over 200 vehicles, which leads to a relatively lower speedup ratio. These differences affect the shapes of their tensor representations and the performance during the best-move identification step.

5.6 Acceleration for different operators

We further examine the TGA method’s performance on different operators, focusing on the speedup gains across benchmark instances of varying sizes. Figure 11 illustrates the speedup ratios of local search operators (*Inter-Relocate*, *Inter-Swap*, *Intra-Relocate*, *Intra-Swap*, 2-opt^* , and 2-opt), calculated as the ratio of the average running time of the traditional CPU implementation in MA to the tensor-based implementation in MA-TGA.

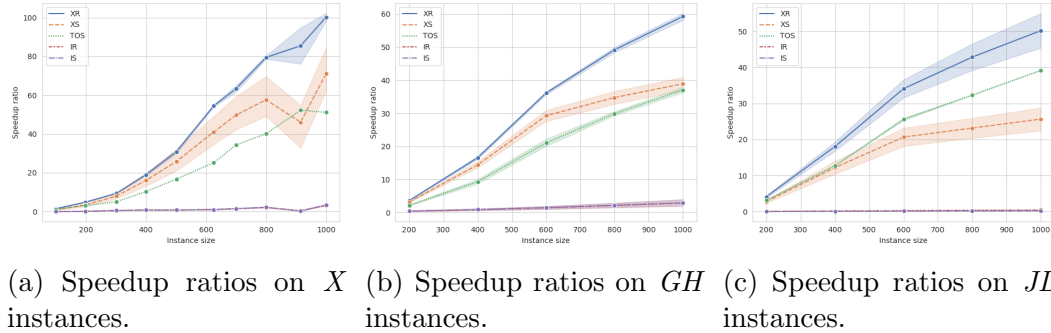


Fig. 11. Speedup ratios for different local search operators: *Inter-Relocate* (XR), *Inter-Swap* (XS), *Intra-Relocate* (IR), *Intra-Swap* (IS), 2-opt^* (TOS), and 2-opt (TO). The x-axis represents the instance size, and the y-axis represents the speedup ratio of the operators indicated by different lines.

Overall, the speedup ratio increases with instance size. In particular, the TGA method shows significant speedups for the inter-route operators (*Inter-Relocate*, *Inter-Swap*, and 2-opt^*). These operators, which involve complex inter-route interactions, benefit greatly from GPU parallelization, achieving speedup ratios ranging from 2 to over 60 for the GH and JD instances, and up to 100 for 1000-node X instance. In comparison, the intra-route operators (*Intra-Relocate*, *Intra-Swap*, and 2-opt) show more modest improvements, with speedup ratios of up to about 2 for large instances with 1000 nodes. This speedup difference highlights the particular advantage of the TGA method for inter-route operators, which require more complex cross-route computations.

5.7 Analysis of key steps in TGA

To complement the theoretical computational complexity analysis provided in Section 4.4, we examine the practical implications of the key steps in the TGA method (Extraction, Concatenation, Difference, Objective, and Update), as defined in Section 4.3, on different operators and instance sizes. Figure 12 illustrates the time consumption of these steps for each operator and instance size.

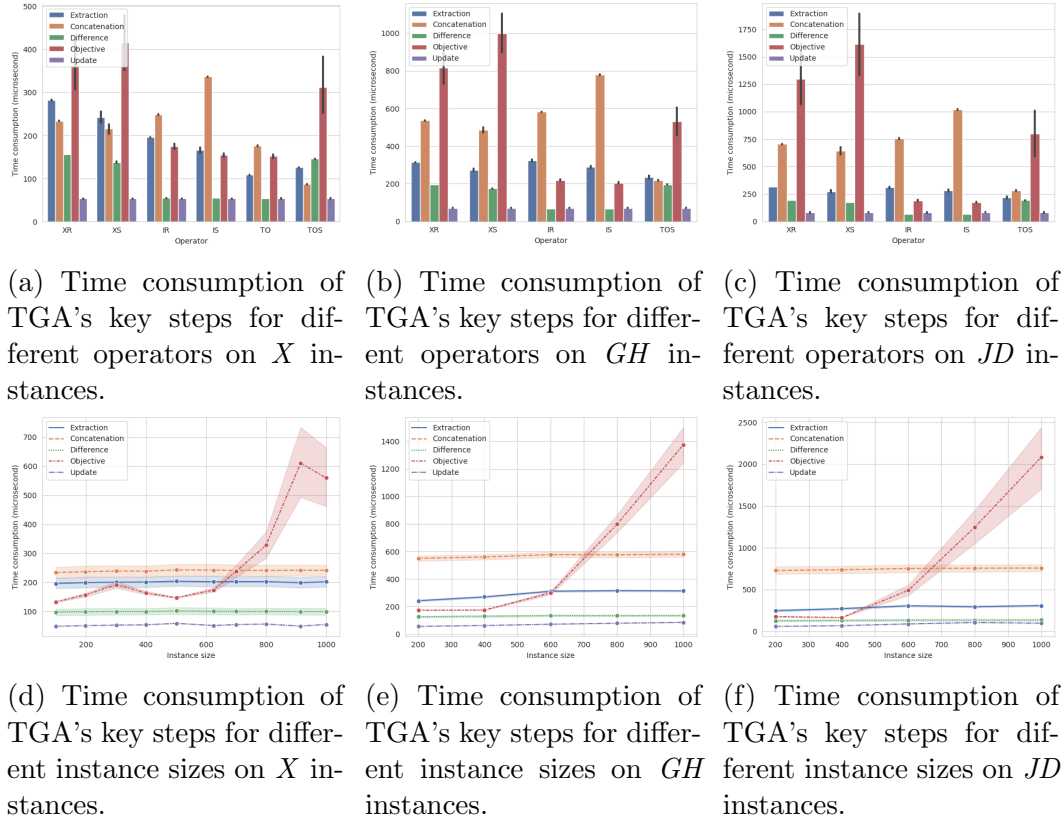


Fig. 12. Analysis of TGA's key steps for different instance sizes and operators: *Inter-Relocate* (XR), *Inter-Swap* (XS), *Intra-Relocate* (IR), *Intra-Swap* (IS), *2-opt** (TOS), and *2-opt* (TO). The x-axis indicates the operators or instance sizes, and the y-axis represents the time consumption of key steps in TGA.

It is observed that most steps (Extraction, Concatenation, Difference, Update) show stable time consumption across different operators and instance sizes, consistent with their near-constant complexity. However, the Objective step's time consumption varies significantly, because it is influenced by the size of the final objective tensor, which depends on instance characteristics like the number of customers, the number of vehicles and maximum route size. This explains the variability of speedup ratios for the X benchmark instances in Figure 10, which shows a negative correlation between the speedup ratio and the time consumption of the Objective step in Figure 12d.

Overall, for the inter-operators, the Objective step is the most time-consuming component due to large neighborhoods and complex inter-route interactions. In contrast, for the intra-operators, smaller neighborhoods reduce the Objective step’s time consumption, but the Concatenation step becomes the bottleneck due to the additional handling of the sequence structures.

This analysis identifies the bottleneck in the proposed TGA method and suggests potential avenues for performance improvement in future work.

5.8 Comparative analysis with algorithms in the literature

Although the primary aim of this study is not to achieve new best-known solutions (BKS) for the benchmark instances, we still provide a comparative analysis of the proposed MA-TGA method against some best existing algorithms from the literature, to offer additional context and reference points. The comparative results are presented in Tables 5-7, corresponding to the X (CVRP), GH (VRPTW), and JD (VRPSPDTW) instances, respectively. Each table includes the instance name, the number of nodes (\mathcal{N}), the best-known solutions (BKS), the best solutions (f) reported by reference algorithms, and the gaps relative to the BKS. For the CVRP and VRPTW, the BKS values are obtained from the CVRPLIB repository (<http://vrp.galagos.inf.puc-rio.br/>) as of April 30, 2025. For the CVRP, we use results from HGS-2012 [38] and HGS-CVRP [14]. For the VRPTW, with the objective of minimizing the total travel distance, we reference results from the DIMACS competition, including both the official DIMACS reference results and the champion team’s algorithm, HGS-DIMACS [39]. For the VRPSPDTW, we report the best results from the state-of-the-art MA-FIRD method [32]. The results of MA-TGA are based on the best solutions obtained in the Section 5.4. The running time limit is comparable for all algorithms.

Table 7 shows that the MA-TGA method achieves competitive results on the tested JD instances, achieving a mean gap of -0.32% relative to the BKS. While the solution quality declines for smaller instances (200 and 400 nodes) due to the removal of the route descent strategy from MA-FIRD, MA-TGA demonstrates clear advantages on larger instances, producing better solutions in short computation times. This outcome is consistent with expectations, as MA-TGA builds on the MA-FIRD framework and integrates the proposed TGA method, which has been proven effective in terms of computational efficiency at larger scales.

For the X (CVRP) and GH (VRPTW) benchmark instances, the performance of the MA-TGA method shows a noticeable gap with the BKS compared to state-of-the-art algorithms. Specifically, MA-TGA yields a mean gap of 1.14%

Table 5

Comparative results on the 10 X benchmark instances of the CVRP between HGS-2012, HGS-CVRP and MA-TGA.

Instance	\mathcal{N}	BKS	HGS-2012		HGS-CVRP		MA-TGA (Best)		
			f	Gap(%)	f	Gap(%)	f	t	Gap(%)
X-n101-k25	100	27591.00	27591.00	0.00	27591.00	0.00	27591.00	286.75	0.00
X-n200-k36	199	58578.00	58578.00	0.00	58578.00	0.00	58755.00	294.60	0.30
X-n303-k21	302	21736.00	21754.00	0.08	21739.00	0.01	21937.00	228.41	0.92
X-n401-k29	400	66154.00	66256.00	0.15	66209.00	0.08	66622.00	377.48	0.71
X-n502-k39	501	69226.00	69264.00	0.05	69230.00	0.01	69675.00	524.58	0.65
X-n627-k43	626	62164.00	62377.00	0.34	62238.00	0.12	63075.00	1039.41	1.47
X-n701-k44	700	81923.00	82302.00	0.46	82075.00	0.19	83580.00	1037.40	2.02
X-n801-k40	800	73305.00	73678.00	0.51	73396.00	0.12	74687.00	1953.10	1.89
X-n916-k207	915	329179.00	329918.00	0.22	329572.00	0.12	332422.00	3601.08	0.99
X-n1001-k43	1000	72355.00	72824.00	0.65	72678.00	0.45	74151.00	3600.03	2.48
MEAN	-	72355.00	86454.20	0.25	86330.60	0.11	87249.50	1294.28	1.14

from the best-known solutions (BKS) on the tested X instances and 0.36% on the tested GH instances. While these results indicate that MA-TGA does not achieve top-tier performance on these benchmarks, this outcome is largely expected and can be reasonably explained by several factors.

First, MA-TGA is built upon the MA-FIRD algorithm, which was originally designed to solve the more complex VRPSPDTW problem. It was not tailored to solve the CVRP or VRPTW, and no algorithmic modifications or parameter tuning were made specifically for these two problem classes in this study. This inevitably affects its competitiveness on these instances.

Second, MA-TGA employs only a limited set of basic local search operators, which are implemented in the TGA method. In contrast, state-of-the-art algorithms typically integrate a richer set of operators and even advanced operators, such as SWAP* [14] and RELOCATE* [39], which significantly enhance solution quality and search capability.

Third, the MA-TGA framework adopts a best-improvement search strategy and does not incorporate neighborhood reduction or pruning techniques. These design choices, made for the sake of experimental consistency and analytical clarity, limit the algorithm's efficiency. In comparison, state-of-the-art algorithms utilize neighborhood reduction strategies such as granular search and pruning techniques to accelerate the search process and improve search efficiency.

Taken together, these factors explain the performance gap observed on the X and GH instances. Nevertheless, MA-TGA still shows competitive behavior and provides a promising basis for further improvement.

Table 6

Comparative results on the 30 *GH* benchmark instances of the VRPTW between BKS, DIMACS, HGS-DIMACS and MA-TGA.

Instance	\mathcal{N}	BKS	DIMACS		HGS-DIMACS		MA-TGA (Best)		
			f	Gap(%)	f	Gap(%)	f	t	Gap(%)
C1.2.1	200	2698.60	2698.60	0.00	2698.60	0.00	2698.60	46.68	0.00
C2.2.1	200	1922.10	1922.10	0.00	1922.10	0.00	1922.10	27.32	0.00
R1.2.1	200	4667.20	4667.20	0.00	4667.20	0.00	4667.20	458.22	0.00
R2.2.1	200	3468.00	3468.00	0.00	3468.00	0.00	3493.70	167.07	0.74
RC1.2.1	200	3516.90	3516.90	0.00	3516.90	0.00	3516.90	592.22	0.00
RC2.2.1	200	2797.40	2797.40	0.00	2797.40	0.00	2799.00	93.35	0.06
C1.4.1	400	7138.80	7138.80	0.00	7138.80	0.00	7138.80	106.94	0.00
C2.4.1	400	4100.30	4100.30	0.00	4100.30	0.00	4100.30	78.91	0.00
R1.4.1	400	10305.80	10305.80	0.00	10305.80	0.00	10330.10	811.28	0.24
R2.4.1	400	7520.70	7520.70	0.00	7520.70	0.00	7558.00	229.05	0.50
RC1.4.1	400	8522.90	8524.00	0.01	8524.00	0.01	8549.70	674.33	0.31
RC2.4.1	400	6147.30	6147.30	0.00	6147.30	0.00	6162.00	223.99	0.24
C1.6.1	600	14076.60	14076.60	0.00	14076.60	0.00	14076.60	119.00	0.00
C2.6.1	600	7752.20	7752.20	0.00	7752.20	0.00	7752.20	110.58	0.00
R1.6.1	600	21274.20	21274.20	0.00	21274.20	0.00	21330.20	2883.36	0.26
R2.6.1	600	15145.30	15145.30	0.00	15145.30	0.00	15281.50	493.77	0.90
RC1.6.1	600	16944.20	16981.30	0.22	16961.10	0.10	17083.20	3690.38	0.82
RC2.6.1	600	11966.10	11979.30	0.11	11966.10	0.00	12010.30	462.35	0.37
C1.8.1	800	25156.90	25156.90	0.00	25156.90	0.00	25156.90	203.70	0.00
C2.8.1	800	11631.90	11631.90	0.00	11632.70	0.01	11632.70	183.16	0.01
R1.8.1	800	36345.00	36393.30	0.13	36465.00	0.33	36718.00	3143.80	1.03
R2.8.1	800	24963.80	24986.80	0.09	24998.90	0.14	25094.30	1302.77	0.52
RC1.8.1	800	29952.80	30039.50	0.29	30058.90	0.35	30141.80	7200.97	0.63
RC2.8.1	800	19201.30	19213.20	0.06	19213.40	0.06	19257.70	666.52	0.29
C1.10.1	1000	42444.80	42444.80	0.00	42444.80	0.00	42444.80	435.31	0.00
C2.10.1	1000	16841.10	16841.10	0.00	16841.10	0.00	16841.10	152.93	0.00
R1.10.1	1000	53026.10	53233.90	0.39	53341.70	0.60	53516.80	6701.68	0.93
R2.10.1	1000	36881.00	36899.40	0.05	36891.30	0.03	37151.80	1994.94	0.73
RC1.10.1	1000	45790.70	45948.50	0.34	46047.30	0.56	46525.90	7200.07	1.61
RC2.10.1	1000	28122.60	28190.80	0.24	28192.10	0.25	28311.60	2900.14	0.67
MEAN	-	17344.09	17366.54	0.06	17375.56	0.08	17442.13	1445.16	0.36

6 Discussion

This section discusses the implications of our findings and the broader applicability of the tensor-based GPU acceleration method for various vehicle routing

Table 7

Comparative results on the 10 *JD* benchmark instances of the VRPSPDTW between BKS, MA-FIRD and MA-TGA.

Instance	\mathcal{N}	BKS	MA-FIRD		MA-TGA (Best)		
			f	Gap(%)	f	t	Gap(%)
F201	200	64083.40	64083.40	0.00	64595.30	376.98	0.80
F203	200	65547.40	65547.40	0.00	65582.70	646.41	0.05
F401	400	115876.00	115876.00	0.00	117199.00	1178.44	1.14
F403	400	115540.00	115540.00	0.00	116288.00	950.51	0.65
F601	600	174108.00	174108.00	0.00	173831.00	1586.54	-0.16
F603	600	177979.00	177979.00	0.00	178120.00	2010.80	0.08
F801	800	208325.00	208325.00	0.00	206932.00	3560.84	-0.67
F803	800	210213.00	210213.00	0.00	209348.00	2745.02	-0.41
F1001	1000	303113.00	303113.00	0.00	296053.00	7200.97	-2.33
F1003	1000	301051.00	301051.00	0.00	293846.00	6508.90	-2.39
MEAN	-	173583.58	173583.58	0.00	172179.50	2676.54	-0.32

problems. We also highlight directions for future research and improvement.

The design of the tensor representation in the TGA method makes it easily extensible to different VRP variants by maintaining attribute matrices tailored to the specific settings and characteristics of the problem. For more complex VRP variants that involve additional decision-making beyond route optimization, such as the multi-depot VRP, the periodic VRP, and the location routing problem, TGA can still be effectively applied to optimize the route optimization component. This flexibility allows TGA to be integrated into existing local search-based VRP frameworks, making it a powerful tool for solving a wide range of VRP variants.

In addition, the TGA method provides a tensor-based implementation for advanced route optimization operators with more complex operations. For example, we can extend basic operators such as *Relocate* and *Swap* to include reverse subsequence operations by swapping the first and last node index tensors of a subsequence, similar to the *2-opt* operator. Moreover, the method supports sequence exchange operations involving more than two routes by introducing additional tensor dimensions to identify the best moves. Additionally, the TGA method can be further improved by incorporating filtering strategies. For example, a mechanism similar to the tabu list can be implemented by using specially designed mask tensors to exclude irrelevant moves. Furthermore, the underlying principles of TGA could also be adapted to other

combinatorial optimization problems, leading to improvements in algorithmic efficiency and computational performance.

However, the TGA method has some limitations and bottlenecks. First, the execution efficiency of the Objective step is affected by the size of the final objective tensor. This could be a major bottleneck if the final objective tensor is of very large size. Also, the TGA method leads to less important speedups for the intra-operators than for the inter-operators. It would be interesting to study additional techniques to improve this situation for the intra-operators. Finally, the current design of the tensor representation of solutions doesn't support easy implementation of pruning strategies and neighborhood reduction techniques that are often used in local search-based routing algorithms. Further research on alternative tensor representations of solutions is needed to make these techniques possible within the proposed TGA framework.

Finally, while TGA offers a promising direction for leveraging GPU parallelism for solving challenging routing problems, it remains an early-stage approach compared to the mature CPU-based implementations. This study focuses on evaluating computational efficiency by implementing basic local search operators with the TGA method. However, rather than directly replicating existing CPU-based search algorithms which are inherently designed and optimized for CPU architectures, future research should aim to design novel search strategies that fully exploit the parallel nature of TGA and GPUs. We believe this approach holds significant potential for advancing the field of combinatorial optimization beyond the limitations of traditional architectures.

7 Conclusion

This work introduces a tensor-based GPU acceleration method for common local search operators in vehicle routing problems. By leveraging fine-grained GPU parallelism, the method significantly speeds up the operator evaluation process.

Extensive experiments on three routing problems, CVRP, VRPTW, and VRP-SPDTW, confirm the effectiveness and efficiency of our proposed method, achieving remarkable performance improvements and computational efficiency gains on benchmark instances compared to traditional CPU-based implementations. In-depth analyses of the acceleration of the studied operators and the key steps within the method provide valuable insights and reveal critical bottlenecks for future improvement.

The proposed TGA method can be seamlessly integrated into various local search-based routing algorithms, providing a powerful and efficient tool for

solving a wide range of vehicle routing problem variants. Its strong extensibility also presents significant potential for further exploration and application. Future research will focus on refining the method and extending it to other combinatorial optimization problems.

Acknowledgments

We acknowledge the support of the HPC resources provided by the Centre de Calcul Intensif des Pays de la Loire (CC IPL), France.

References

- [1] G. B. Dantzig, J. H. Ramser, The truck dispatching problem, *Management Science* 6 (1) (1959) 80–91.
- [2] G. Clarke, J. W. Wright, Scheduling of vehicles from a central depot to a number of delivery points, *Operations Research* 12 (4) (1964) 568–581.
- [3] J. K. Lenstra, A. Rinnooy Kan, Complexity of scheduling under precedence constraints, *Operations Research* 26 (1) (1978) 22–35.
- [4] G. Laporte, The vehicle routing problem: An overview of exact and approximate algorithms, *European Journal of Operational Research* 59 (3) (1992) 345–358.
- [5] J. Andelmin, E. Bartolini, An exact algorithm for the green vehicle routing problem, *Transportation Science* 51 (4) (2017) 1288–1303.
- [6] R. Praxedes, T. Bulhões, A. Subramanian, E. Uchoa, A unified exact approach for a broad class of vehicle routing problems with simultaneous pickup and delivery, *Computers & Operations Research* 162 (2024) 106467.
- [7] W.-C. Chiang, R. A. Russell, Simulated annealing metaheuristics for the vehicle routing problem with time windows, *Annals of Operations Research* 63 (1996) 3–27.
- [8] E. Rodríguez-Esparza, A. D. Masegosa, D. Oliva, E. Onieva, A new hyperheuristic based on adaptive simulated annealing and reinforcement learning for the capacitated electric vehicle routing problem, *Expert Systems with Applications* 252 (2024) 124197.
- [9] P. Toth, D. Vigo, The granular tabu search and its application to the vehicle-routing problem, *Inform Journal on Computing* 15 (4) (2003) 333–346.
- [10] M. Gmira, M. Gendreau, A. Lodi, J.-Y. Potvin, Tabu search for the time-dependent vehicle routing problem with time windows on a road network, *European Journal of Operational Research* 288 (1) (2021) 129–140.

- [11] B. M. Baker, M. Ayechev, A genetic algorithm for the vehicle routing problem, *Computers & Operations Research* 30 (5) (2003) 787–800.
- [12] A. S. Tasan, M. Gen, A genetic algorithm based approach to vehicle routing problem with simultaneous pick-up and deliveries, *Computers & Industrial Engineering* 62 (3) (2012) 755–761.
- [13] D. Cattaruzza, N. Absi, D. Feillet, T. Vidal, A memetic algorithm for the multi trip vehicle routing problem, *European Journal of Operational Research* 236 (3) (2014) 833–848.
- [14] T. Vidal, Hybrid genetic search for the cvrp: Open-source implementation and swap* neighborhood, *Computers & Operations Research* 140 (2022) 105643.
- [15] G. Laporte, Fifty years of vehicle routing, *Transportation Science* 43 (4) (2009) 408–416.
- [16] T. Vidal, T. G. Crainic, M. Gendreau, C. Prins, Heuristics for multi-attribute vehicle routing problems: A survey and synthesis, *European Journal of Operational Research* 231 (1) (2013) 1–21.
- [17] K. Braekers, K. Ramaekers, I. Van Nieuwenhuysse, The vehicle routing problem: State of the art classification and review, *Computers & Industrial Engineering* 99 (2016) 300–313.
- [18] S.-Y. Tan, W.-C. Yeh, The vehicle routing problem: State-of-the-art classification and review, *Applied Sciences* 11 (21) (2021) 10295.
- [19] J. D. Owens, M. Houston, D. Luebke, S. Green, J. E. Stone, J. C. Phillips, Gpu computing, *Proceedings of the IEEE* 96 (5) (2008) 879–899.
- [20] M. H. Rashid, I. McAndrew, An efficient gpu framework for parallelizing combinatorial optimization heuristics, in: *2020 International Conference on Advances in Computing and Communication Engineering, IEEE, 2020*, pp. 1–7.
- [21] J. R. Cheng, M. Gen, Accelerating genetic algorithms with gpu computing: A selective overview, *Computers & Industrial Engineering* 128 (2019) 514–525.
- [22] O. Goudet, J.-K. Hao, A massively parallel evolutionary algorithm for the partial latin square extension problem, *Computers & Operations Research* 158 (2023) 106284.
- [23] O. Goudet, A. Goëffon, J.-K. Hao, A large population island framework for the unconstrained binary quadratic problem, *Computers & Operations Research* 168 (2024) 106684.
- [24] B. Nogueira, W. Rosendo, E. Tavares, E. Andrade, Gpu tabu search: a study on using gpu to solve massive instances of the maximum diversity problem, *Journal of Parallel and Distributed Computing* (2024) 105012.
- [25] M. F. Abdelatti, M. S. Sodhi, An improved gpu-accelerated heuristic technique applied to the capacitated vehicle routing problem, in: *Proceedings of the 2020 Genetic and Evolutionary Computation Conference, 2020*, pp. 663–671.

- [26] Z. Zhang, Y. Sun, H. Xie, Y. Teng, J. Wang, Gmma: Gpu-based multiobjective memetic algorithms for vehicle routing problem with route balancing, *Applied Intelligence* 49 (2019) 63–78.
- [27] C. Schulz, Efficient local search on the gpu—investigations on the vehicle routing problem, *Journal of Parallel and Distributed Computing* 73 (1) (2013) 14–31.
- [28] P. Yelmewad, B. Talawar, Gpu-based parallel heuristics for capacited vehicle routing problem, in: *2020 IEEE International Conference on Electronics, Computing and Communication Technologies, IEEE*, 2020, pp. 1–6.
- [29] I. Coelho, P. Munhoz, L. S. Ochi, M. Souza, C. Bentes, R. Farias, An integrated cpu–gpu heuristic inspired on variable neighbourhood search for the single vehicle routing problem with deliveries and selective pickups, *International Journal of Production Research* 54 (4) (2016) 945–962.
- [30] T. Vidal, T. G. Crainic, M. Gendreau, C. Prins, A unified solution framework for multi-attribute vehicle routing problems, *European Journal of Operational Research* 234 (3) (2014) 658–673.
- [31] S. Liu, K. Tang, X. Yao, Memetic search for vehicle routing with simultaneous pickup-delivery and time windows, *Swarm and Evolutionary Computation* 66 (2021) 100927.
- [32] Z. Lei, J.-K. Hao, A memetic algorithm for vehicle routing with simultaneous pickup and delivery and time windows, *IEEE Transactions on Evolutionary Computation (Early Access)*, DOI: 10.1109/TEVC.2024.3456585 (2024) 1–1.
- [33] Y. Nagata, O. Bräysy, W. Dullaert, A penalty-based edge assembly memetic algorithm for the vehicle routing problem with time windows, *Computers & Operations Research* 37 (4) (2010) 724–737.
- [34] T. Vidal, T. G. Crainic, M. Gendreau, C. Prins, A hybrid genetic algorithm with adaptive diversity management for a large class of vehicle routing problems with time-windows, *Computers & Operations Research* 40 (1) (2013) 475–489.
- [35] E. Uchoa, D. Pecin, A. Pessoa, M. Poggi, T. Vidal, A. Subramanian, New benchmark instances for the capacitated vehicle routing problem, *European Journal of Operational Research* 257 (3) (2017) 845–858.
- [36] H. Gehring, J. Homberger, A parallel hybrid evolutionary metaheuristic for the vehicle routing problem with time windows, in: *Proceedings of EUROGEN99, Vol. 2*, Springer, 1999, pp. 57–64.
- [37] F. Wilcoxon, Individual comparisons by ranking methods, in: *Breakthroughs in statistics: Methodology and distribution*, Springer, 1992, pp. 196–202.
- [38] T. Vidal, T. G. Crainic, M. Gendreau, N. Lahrichi, W. Rei, A hybrid genetic algorithm for multidepot and periodic vehicle routing problems, *Operations Research* 60 (3) (2012) 611–624.

- [39] W. Kool, J. O. Juninck, E. Roos, K. Cornelissen, P. Agterberg, J. van Hoorn, T. Visser, Hybrid genetic search for the vehicle routing problem with time windows: A high-performance implementation, in: 12th DIMACS Implementation Challenge Workshop, DIMACS, Rutgers University Piscataway, NJ, 2022.